



HAL
open science

Molecular content of nascent soot: Family characterization using two-step laser desorption laser ionization mass spectrometry

Hassan Sabbah, Mario Commodo, Francesca Picca, Gianluigi de Falco, Andrea d'Anna, Patrizia Minutolo, Andrea d'Anna, Christine Joblin

► To cite this version:

Hassan Sabbah, Mario Commodo, Francesca Picca, Gianluigi de Falco, Andrea d'Anna, et al.. Molecular content of nascent soot: Family characterization using two-step laser desorption laser ionization mass spectrometry. Proceedings of the Combustion Institute, 2020, 38 (1), pp.1241-1248. 10.1016/j.proci.2020.09.022 . hal-03007513

HAL Id: hal-03007513

<https://hal.science/hal-03007513>

Submitted on 16 Nov 2020

HAL is a multi-disciplinary open access archive for the deposit and dissemination of scientific research documents, whether they are published or not. The documents may come from teaching and research institutions in France or abroad, or from public or private research centers.

L'archive ouverte pluridisciplinaire **HAL**, est destinée au dépôt et à la diffusion de documents scientifiques de niveau recherche, publiés ou non, émanant des établissements d'enseignement et de recherche français ou étrangers, des laboratoires publics ou privés.

1 **MOLECULAR CONTENT OF NASCENT SOOT: FAMILY**
2 **CHARACTERIZATION USING TWO-STEP LASER DESORPTION LASER**
3 **IONIZATION MASS SPECTROMETRY**

4
5 Hassan Sabbah ^a, Mario Commodo ^b, Francesca Picca ^c, Gianluigi de Falco ^c

6 Patrizia Minutolo ^b, Andrea D'Anna ^{c,*}, Christine Joblin ^{a,*}

7
8 ^a Institut de Recherche en Astrophysique et Planétologie (IRAP), Université de Toulouse (UPS),
9 CNRS, CNES, 9 Av. du Colonel Roche, 31028 Toulouse Cedex 4, France

10 ^b Istituto di Ricerche sulla Combustione, CNR, P.le Tecchio 80, 80125, Napoli, Italy

11 ^c Dipartimento di Ingegneria Chimica, dei Materiali e della Produzione Industriale - Università
12 degli Studi di Napoli Federico II, P.le Tecchio 80, 80125, Napoli, Italy

13
14 * Corresponding Authors: Andrea D'Anna anddanna@unina.it

15 Christine Joblin christine.joblin@irap.omp.eu

16
17
18
19 **Colloquium: SOOT, NANOPARTICLES, PAH AND OTHER LARGE MOLECULES**
20
21
22
23

24 ABSTRACT

25 Molecules constituting nascent soot particles have been analyzed by two-step laser desorption laser
26 ionization mass spectrometry. Three samples have been collected from a slightly sooting ethylene/air
27 premixed flame with the aim to investigate soot composition in the transition from nucleated to just-
28 grown soot particles. Sampling locations have been selected based on the evolution of the particle
29 size distribution along the flame axis. The mass spectrometric results point to a strong evolution of
30 the molecular composition. Just-nucleated soot is rich in polycyclic aromatic hydrocarbons (PAHs)
31 dominated by medium sizes from 18 to 40 carbon atoms but containing sizes as large as 90 carbon
32 atoms. Most abundant PAHs are in the form of *peri*-condensed structures. The presence of a large
33 fraction of odd numbered carbon species shows that pentagonal cycles are a common feature of the
34 detected population. Increasing the distance from the burner outlet, i.e., the particle residence time in
35 flame, leads to an evolution of the chemical composition of this population with a major contribution
36 of carbon clusters including also fullerenes up to about 160 carbon atoms. Our data support a scenario
37 in which large PAHs containing pentagonal rings evolve very efficiently upon thermal processing by
38 a series of dehydrogenation and isomerization processes to form fullerenes. This chemistry happens
39 in the early steps of soot growth showing that carbonization is already active at this stage.

40

41 KEYWORDS

42 Soot; early growth; carbonization; molecular composition; polycyclic aromatic hydrocarbons;
43 fullerenes; laser mass spectrometry.

44 1. INTRODUCTION

45 Soot nucleation and early growth in flames has been subject of intense discussion for a long time.
46 The elusive nature of the soot formation mechanism is due to the complexity of the involved chemical
47 and physical processes; these include high-temperature pyrolysis and gas-phase oxidation chemistry,
48 polycyclic aromatic hydrocarbon (PAH) formation, particle nucleation followed by particle growth
49 through coagulation/coalescence and heterogeneous surface reactions. Particle agglomeration, in
50 addition to carbonization/dehydrogenation and oxidation reactions, further contributes to the final
51 shape and structure of the generated particles. As a result, soot particles evolve in flames by changing
52 size, chemical composition and structural order.

53 The term nascent soot refers to the soot particles during the early stages of the formation process
54 [1], which includes just-nucleated (incipient) to just-grown soot particles. In a laminar premixed
55 flame of an aliphatic hydrocarbon, soot nucleates right after the flame front [2], resulting in the
56 formation of a unimodal particle size distribution (PSD) with a maximum number density for particles
57 of 2-3 nm [3-6]. Once formed, incipient soot undergoes size growth via coagulation/coalescence
58 processes and surface chemical reactions with gas-phase molecules. This next step results in the
59 formation of a second, and larger in size, particle mode whose mean diameter increases as a function
60 of residence time [3-6]. During the growing/aging process in flame, soot is known to carbonize, thus
61 resulting in a lowering of H/C ratio down to the very low value of 0.1 typically associated to mature
62 soot [7,8].

63 Mass spectrometry techniques (*in situ* and *ex situ*) have contributed significantly to our
64 understanding of the chemistry involved in soot formation and growth [9,10]. Laser
65 desorption/ionization (LDI) techniques [11,12], particularly sensitive to PAHs [13], succeeded to give
66 a comprehensive view of the soot molecular composition during the transition from gaseous phase to
67 solid particles. In order to follow the evolution of the molecular constituents of the particles during
68 the early stages of particle transformation, we have performed two-step laser desorption laser
69 ionization mass spectrometry (L2MS) of the nascent soot particles collected from a slightly sooting

70 ethylene/air laminar premixed flame. The study is aimed at shedding light on the molecular content
71 and its variation with evolving chemical and physical conditions.

72

73 2. EXPERIMENTAL

74 2.1 *Flame and soot sampling*

75 Soot particles were sampled from an ethylene/air laminar premixed flame stabilized on a McKenna
76 burner. The cold gas velocity was set to 9.8 cm/s (STP) and the carbon to oxygen (C/O) ratio was
77 0.67. The particle sampling system for on-line and off-line soot analysis has been described in earlier
78 works [3,14,15]. Briefly, soot was sampled from the flame through an orifice (diameter=0.2 mm,
79 thickness = 0.5 mm) in a tubular dilution probe (outer diameter=1 cm), positioned horizontally in the
80 flame. The sampled mixture was immediately diluted with N₂ to quench chemical reactions and
81 minimize particle aggregation [5]. For the off-line analysis, a stainless-steel aerosol filter holder
82 containing a 25 mm pure silver membrane filter (Millipore-AG4502550) was positioned on-line
83 downstream of the dilution tubular probe for soot nanoparticles collection.

84

85 2.2 *Mass Spectrometry Analysis*

86 AROMA (Aromatic Research of Organics with Molecular Analyzer) is an experimental setup that
87 combines laser desorption ionization techniques (LDI) to a segmented linear quadrupole ion trap
88 connected to an orthogonal time of flight mass spectrometer (LQIT-oTOF). [16]. A sketch of the
89 AROMA system (Fig.S1) as well as detailed experimental conditions and performances are reported
90 in the supplementary materials. Mass spectrometry data and chemical analysis tools for all the studied
91 samples are made publicly available in the AROMA database: <http://aroma.irap.omp>. AROMA was
92 successfully used to characterize, with high sensitivity (down to attomole), PAHs molecular
93 distribution in Murchison meteorite [16]. Recently [17,18], we have shown the ability of AROMA to

94 track the chemical evolution of carbonaceous molecules involved in the formation of cosmic dust
95 analogues produced from a carbon vapor (C, C₂) and in the presence of H₂ or C₂H₂.

96 For this work, particles collected on the filter have been analyzed using the well-established and
97 optimized two-step laser mass spectrometry (L2MS) scheme. In this scheme, desorption and
98 ionization are clearly separated and optimized in time and space and performed with two different
99 pulsed (5 ns of pulse duration) lasers. During the desorption step, an infrared laser (Nd:YAG at
100 1064 nm) is focused on the sample with a spot size of 300 μm producing a fluence of desorption E_d
101 = 150 mJ/cm². As discussed in the supplementary materials, these conditions ensure thermal
102 desorption avoiding ablation and chemistry in the plume. This implies that the detected molecules
103 come from the surface of the particles with contribution from their volume if these particles consist
104 of loosely bound components. Ionization is performed by intercepting perpendicularly the expanding
105 plume of the desorbed molecules using an ultraviolet laser (fourth harmonic of an Nd:YAG at 266
106 nm). This scheme presents a high selectivity and sensitivity for species that can undergo (1+1)
107 resonance-enhanced multiphoton ionization (REMPI) such as PAHs and fullerenes [19,20]. The used
108 laser ionization fluence is $E_i=16$ mJ/cm².

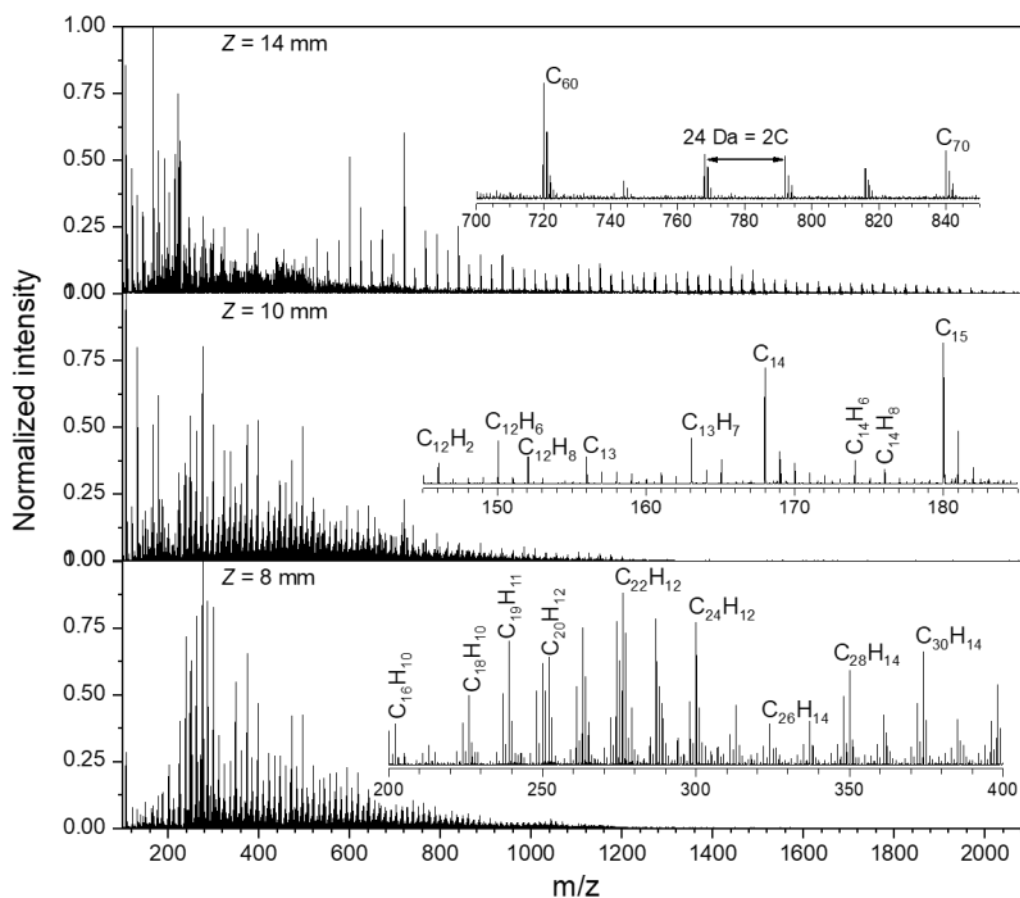
109

110 3. RESULTS AND DISCUSSION

111 The evolution of the particle size distributions in number concentrations for the flame herein
112 investigated, measured along the flame at different burner-to-probe separation distances (Z), has been
113 reported in Ref. 15 (Fig. 1). In the present work three different conditions, i.e., different Z , have been
114 selected for soot sampling and characterization via L2MS-TOF, namely 8, 10 and 14 mm, whose
115 corresponding size distributions in volume are reported in Fig. S2 in the supplementary materials.
116 The PSD in volume develops from a single mode with the most abundant particles having a size of
117 3.5 nm at $Z = 8$ mm, to a bimodal size distribution where in addition to such incipient particle mode
118 a larger mode made of just-grown soot particles with mobility diameter in the range of 5-15 nm is
119 present at $Z = 10$ mm, and finally to a condition in which most of the mass is in the second mode with

120 a maximum corresponding to particles with mobility diameter of approximately 20 nm at $Z = 14$
121 mm. It is worth noticing that for this last condition, the PSD is bimodal if plotted in number, with a
122 first particle mode centered at approximately 2.4 nm (roughly as the ones measured at 8 and 10
123 mm). However, this mode is not observable in Fig. S2 because of the very low mass of such particles
124 [3].

125 The mass spectra of the three soot samples are reported in Fig.1 for the 100-2000 m/z range. Three
126 different inset zoom graphs are also sketched with different mass ranges. Molecular mass for the
127 incipient soot particles ($Z = 8$ mm) spans over all the studied range, with the most intense peaks falling
128 in the 200-700 m/z range with a mean weighted mass of $m/z = 447$. Several early studies have led to
129 the observations that nascent soot particles are mainly composed by PAHs of moderate size (about
130 the size of ovalene) [14,15,21], a result which is also consistent with other previous mass
131 spectrometric investigations in similar flame conditions [13,22]. Although, the measurements herein
132 presented are in good agreement with these previous observations, they indicate slightly larger value
133 of the mean molecular mass distribution of the aromatic constituents (C_{36} on average); a result
134 however in closer agreement with the recent LD-MS investigation of soot reported by Jacobson et al.
135 [11]. The PAH distribution obtained in our study spans a large size range with detected species up to
136 about 90 carbon atoms. In addition, peaks corresponding to PAHs having an odd number of carbon
137 atoms from C_9 to C_{91} are measured, some with a strong intensity (e.g., $C_{19}H_{11}$, $C_{21}H_{11}$, $C_{23}H_{11}$).



138

139 Fig.1. Mass spectra at three burner-to-probe distances, i.e., $Z = 8$ mm, $Z = 10$ mm and $Z = 14$ mm,
 140 characteristic of the transition from incipient to just-grown soot particles. Fluences of $E_d = 150$
 141 mJ/cm^2 and $E_i = 16 \text{ mJ}/\text{cm}^2$ have been used for the desorption (1064 nm) and ionization (266 nm)
 142 lasers, respectively. Peak annotations are given for corresponding neutral species. Inset zoom graph
 143 at $Z = 8$ mm presents some of the species detected over the (200-400) m/z range. At $Z = 10$ mm the
 144 inset zoom graph shows the co-existence of aromatic species with carbon clusters. At $Z = 14$ mm the
 145 inset zoom graph presents the detection of fullerenes over the (700-840) m/z range. ^{13}C isotopologs
 146 are clearly seen in this zoom.

147

148 The mass spectrum for soot collected at $Z = 14$ mm exhibits significant differences. The PAH
 149 distribution is shifted to lower mass with a mean at $m/z = 300$ compared to $m/z = 447$ at $Z = 8$ mm. In
 150 addition, a series of peaks attributed to pure carbon species (C_x) clearly appears. In the low mass
 151 range they are found for each carbon atom numbers, e.g., C_9 , C_{10} , C_{11} up to C_{21} . This is followed by
 152 a jump to C_{30} from which a series starts separated by 2C up to C_{160} . The most intense peaks are found
 153 for C_{60} ($m/z = 720$), C_{50} , C_{52} and C_{70} , which suggest that they correspond to fullerenes [23].

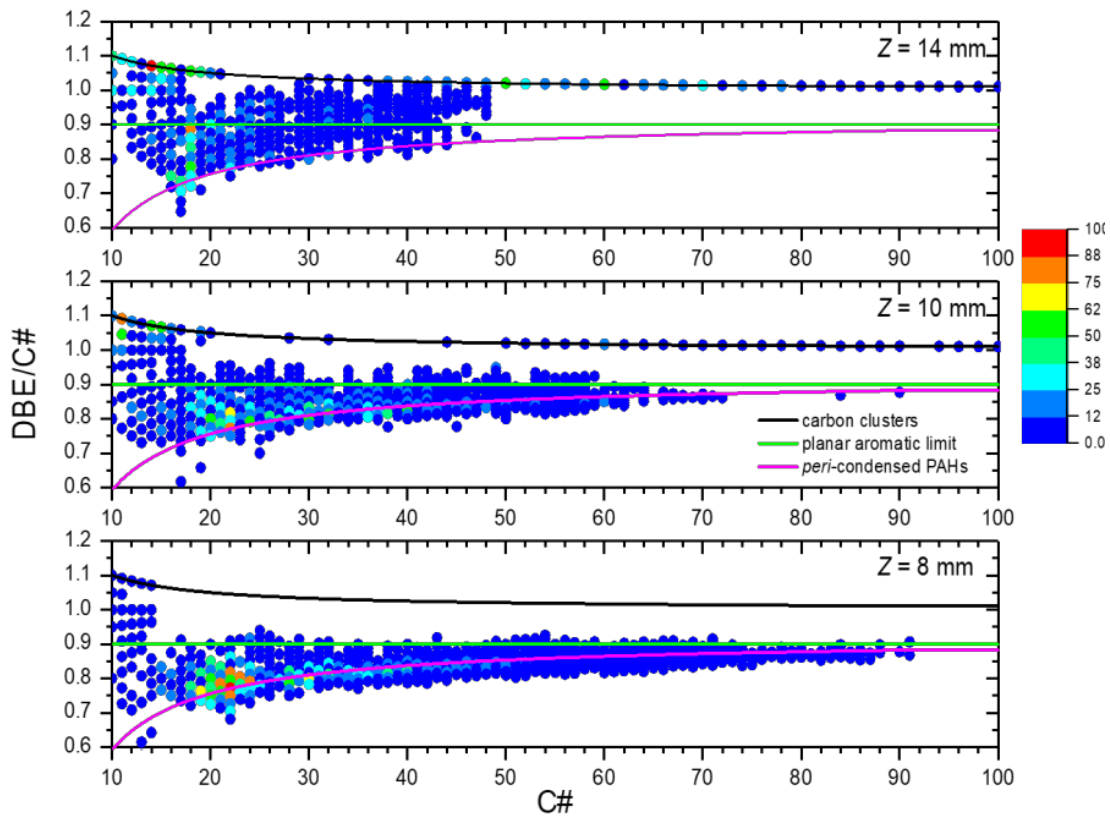
154 C clusters have been reported by Dobbins et al. [24] for high heights above the burner, using LDI
155 in single step with a 266 nm-laser and an irradiance of 1-20 MW/cm². Homann [25], has detected
156 fullerenes in premixed low-pressure flames by on line analysis. The author reported that the formation
157 of fullerenes relative to soot can be so low that these species can only be detected with the most
158 sensitive analytical techniques. Our L2MS technique uses a REMPI scheme, which provides very
159 high sensitivity and was also the one used in Homann's experiments [25]. Our detection is not
160 surprising from this point of view. In addition, we report an evolution with increasing Z both in
161 chemical complexity and in molecular families. The data at position $Z = 10$ mm show an intermediate
162 case in which carbon clusters start to be representative in the mass spectrum. We note that Jacobson
163 et al. [11] could not observe these species, possibly pointing to different sampled flame conditions.

164 It is worth to note, that the overall intensity of the mass spectra lowers as Z increases. This factor
165 is respectively 1.8 and 3.5 for $Z=10$ and 14 mm compared to $Z=8$ mm. This likely reflects a change
166 in the molecular components of the particles, which results in a lower production of molecules upon
167 laser desorption as also noticed in our previous study [15]. In addition, a number of 684, 591 and 463
168 species have been identified for $Z=8$, 10 and 14 mm respectively, which shows that the molecular
169 diversity is changing as well. We will discuss in the following that the probed molecules have been
170 subject to processing which favors the most stable species such as fullerenes.

171 Some chemical species with one or two oxygen atoms have been observed for samples at $Z = 8$
172 and $Z = 10$ mm. In each sample about 20 peaks of molecules containing oxygen are identified with
173 an average m/z precision <0.01 (see Table S4). The total ion signal from oxygenated compounds
174 represents 1% from the total ion signal at $Z=8$ and 3% at $Z=10$ mm. This low level is consistent with
175 LDI-MS measurements of soot extracted from a diffusion flame [11]. One has to be careful though
176 not to translate this number into an abundance ratio due to the bias of our technique. We note though
177 that evidences of few atomic oxygen percentages in nascent soot were observed by photoemission
178 experiments [26].

179 In order to obtain a more in-depth evaluation of the aromaticity of the molecular constituents of
 180 the nascent soot particles we performed the double bond equivalent (DBE) analysis [16] of the species
 181 on the bases of the measured mass spectra. The DBE value is defined by $DBE = C\# - H\#/2 + N\#/2 +$
 182 1 with $C\#$, $H\#$ and $N\#$, the numbers of C, H and N atoms inside the molecules. It is representative of
 183 the unsaturation level of the molecules and thus corresponds to a direct measure of their aromaticity.
 184 More details about DBE are provided in the supplementary materials.

185 Colored map plots presenting the calculated $DBE/C\#$ values as a function of $C\#$ are reported in
 186 Fig.2 for the three samples. The color scale is the relative intensity (normalized to the highest peak
 187 in the spectrum) of each species in the mass spectrum.



188
 189 Fig.2. Colored map plots of $DBE/C\#$ vs. carbon number ($C\#$) constructed from the molecular
 190 formulas which have been derived from the mass spectra of soot sampled at $Z = 8, 10$ and 14 mm.
 191 The color scale is representative of the relative intensity (normalized to the highest peak in the
 192 spectrum) for each identified species. Black line refers to carbon clusters ($DBE = n(C) + 1$); green
 193 line refers to the planar aromatic limit ($DBE = 0.9 * C\#$) [28], and magenta line refers to the purely
 194 *peri*-condensed PAHs (most compact structures made of 6-member rings) with $DBE = -3.24 +$
 195 $0.92 * C\#$.
 196

197 At $Z=8$ mm, the DBE/C# values are mainly distributed below the planar aromatic limit line (green
198 line), based on the classification of petroleum components [27,28]. For a given number of C atoms,
199 a quite narrow distribution of H atoms is measured with a relevant fraction of aromatic molecules
200 having a molecular structure with a number of H-atoms larger than that corresponding to the most
201 *peri*-condensed structure (magenta line). Still all species stay close to this line, which shows that their
202 structures are compact and do not contain much aliphatic bonds. This statement is strictly valid for
203 PAHs containing 6-membered rings only. Indeed, the introduction of 5-membered rings increases the
204 unsaturation. For instance, the formula $C_{24}H_{12}$ can correspond to the most *peri*-condensed structure
205 coronene, but also to a less compact structure with 2 pentagonal rings as imaged by Commodo et al.
206 [15].

207 Our results differ from those of earlier studies that concluded about the importance of aliphatic
208 components in the PAH population [29] but is consistent with the more recent study of Jacobson et
209 al. [11].

210 The DBE/C# values, corresponding to the chemical composition of just-grown soot particles at
211 $Z = 14$ mm, mainly stand above the planar aromatic limit showing an increase of the degree of
212 unsaturation and even the formation of structures with very low hydrogen content. Another important
213 change in the molecular composition between $Z=14$ and $Z=8$ mm concerns the highest mass range.
214 From $C\#=50$ and above, 326, 185 and 59 species are detected at $Z=8$, 10 and 14 mm, respectively.
215 These large species are exclusively fullerenes at $Z=14$ mm, but none of them are fullerenes at
216 $Z=8$ mm.

217 The DBE method allows us to segregate the derived molecular formulas into families. We consider
218 the value of $DBE/C\# = 0.9$ as the limit of planar aromatics as defined in Ref. [28]. DBE/C# values
219 below 0.9 correspond to aromatic species with less condensed structures, including potential cross-
220 linked aromatics, and/or the presence of aliphatic CH bonds. DBE/C# values above 0.9 and below 1
221 correspond to less hydrogenated species that we call HC clusters. In addition, we consider a family
222 of C clusters for $C\#<30$ and fullerenes above [23].

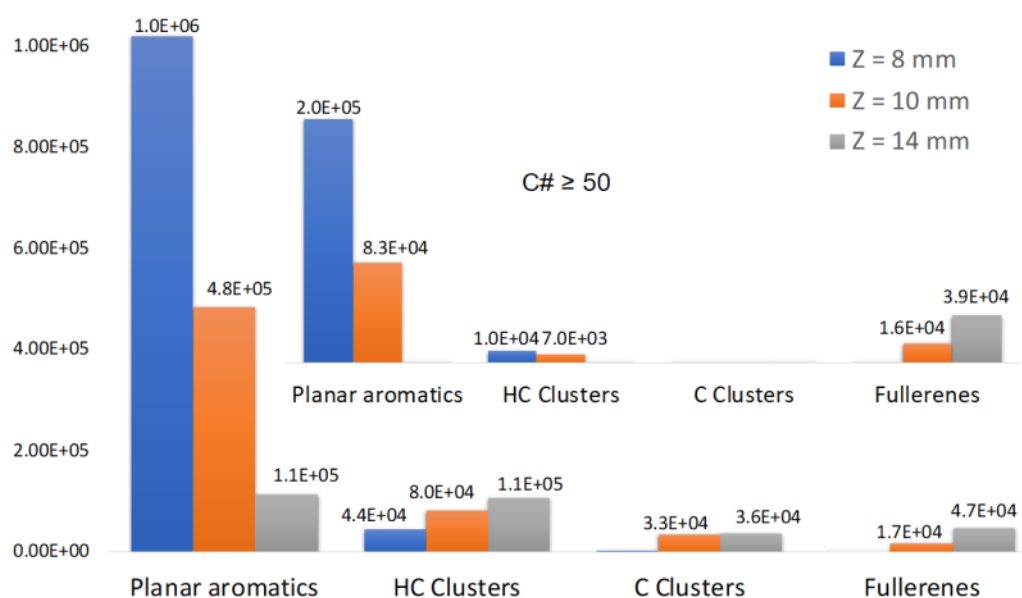
223

224 Table 1. Evolution of the family composition as a function of Z derived from a DBE analysis of the
 225 mass spectra in Fig. 1. Sum of relative peak intensities and mean mass (m/z) weighted by peak
 226 intensities in parenthesis.

| Family composition | | | | |
|--------------------|------------------|---------------|---------------|---------------|
| Sample | Planar aromatics | HC Clusters | C Clusters | Fullerenes |
| $Z = 8$ mm | 0.96 (447.30) | 0.04 (376.16) | 0.00 | 0.00 |
| $Z = 10$ mm | 0.79 (432.15) | 0.13 (338.90) | 0.05 (164.22) | 0.03 (805.02) |
| $Z = 14$ mm | 0.38 (300.83) | 0.33 (337.36) | 0.13 (178.14) | 0.16 (874.30) |

227

228



229

230 Fig.3. Evolution of the molecular families derived from the mass spectra after DBE analysis.

231

232 Our results show that molecular constituents associated with soot particles change in the passage
 233 from the first particle mode at 3.5 nm to the second mode at 9 nm (see Fig.S2). The analysis in
 234 molecular families suggests a transition in the population from PAHs to HC clusters and even to
 235 fullerenes along the flame (Fig.3). Indeed, when just-grown soot particles are formed, i.e., $Z=14$ mm,
 236 the few large molecules ($C\#\geq 50$) detached from the particles are found in fullerenes indicating that
 237 soot transformation is accompanied by a strong dehydrogenation process of large carbonaceous
 238 molecules.

239 To further explore the molecular family change across the particle growing process we have
240 analyzed in more details the DBE/C# vs C# at Z=8 mm and 14 mm as reported in Fig. S3. At Z=8 mm,
241 the dominant PAH species contain C# = 20-24 (see Fig. 2) and a typical number of hydrogens of 10
242 or 12, which points to a dominant population of compact structures and structures with a few
243 pentagonal rings as discussed above for C₂₄H₁₂. As C# increases in the PAH species, the number of
244 hydrogens only slightly increases reaching a maximum of 20 for species larger than 40 carbons. This
245 leads to a growth scheme by a global C₂/C₂H addition, which can be obtained by C₂H₂/C₂H addition
246 and hydrogen removal as postulated in the HACA mechanism [30].

247 The formation of species with an odd number of C atoms is expected to arise from reactivity with
248 oxygen [25] and also addition of C/CH as suggested in [31,32]. These processes can form pentagonal
249 cycles at the periphery of PAHs. An analysis of the odd-numbered species was performed amongst
250 the population of planar aromatics (DBE/C#≤0.9). At Z=8 mm, the odd C number species represent
251 49% of the peak numbers of which 67% are odd H containing species. The latter number is
252 significantly larger than the total of 48% for these species in the sample. This is consistent with odd
253 C containing PAH species with odd H number corresponding to π radicals. The delocalization of the
254 charge in these ions further contributes to their stability. These odd-numbered structures can include
255 both species with pentagonal ring(s) and some made solely of six-membered rings [25]. At Z = 14
256 mm, the odd hydrogen-containing species sum up to 48% of all the intensity but up to 70% when only
257 odd C containing species (44% of the population) are considered. These numbers appear to be
258 consistent with the value at Z=8 mm suggesting that π radicals constitute a significant fraction of the
259 molecular population.

260 Concerning the even C number species, mildly dehydrogenated species are observed at Z=8 mm.
261 For instance, the intensity of C₂₄H₁₀ is significant (0.45 that of C₂₄H₁₂) The presence of less
262 hydrogenated species is confirmed also for large PAHs (see Fig.S3). For instance, for C#=42, the
263 most compact *peri*-condensed structure would correspond to circumpyrene (C₄₂H₁₆). Still species
264 corresponding to a lower number of H, in particular C₄₂H₁₄ and C₄₂H₁₂ are observed. Similarly,

265 circumcoronene ($C_{54}H_{18}$) is detected together with $C_{54}H_{16}$ and $C_{54}H_{14}$. At $Z = 14$ mm, the intensity of
266 $C_{24}H_{10}$ is 1.5 times higher compared to coronene and we observe much strongly dehydrogenated
267 species (e.g. $C_{24}H_4$, $C_{24}H_6$).

268 Pure PAHs are expected to exhibit only minor fragmentation during the analysis with AROMA
269 [16]. We therefore consider that these species which contain less hydrogens are intrinsic to the sample
270 and not formed in our analysis. The addition of C_2 can form pentagonal cycles mainly leading to
271 acenaphthylene-type compounds, which can also be found in dehydrogenated form (1,2-dehydro-
272 acenaphthylene; $C_{12}H_6$). In the $Z=8$ mm sample the ratio $C_{12}H_6/C_{12}H_8$ is equal to 2.3. This might be
273 an explanation for the large intensity of species with mild dehydrogenation (typically 2H below the
274 H number of the most compact *peri*-condensed structures). The presence of pentagonal rings inside
275 the carbon structure is also expected. $C_{20}H_{10}$, which would correspond to the bowl-shaped
276 corannulene molecule, has a similar peak intensity as $C_{20}H_{12}$, which would correspond to the full six-
277 membered rings. Therefore, the observed population with low hydrogen content likely reveals the
278 formation of species containing an increasing number of pentagonal cycles. Structures containing
279 several pentagonal cycles are predicted to be the most abundant structures at high temperatures in
280 thermodynamic equilibrium (e.g. $C_{30}H_{10}$ with 6 pentagonal rings and 5 hexagonal rings as predicted
281 by [33]). These pentagonal structures induce some strain that can be release by closing the structure
282 towards fullerenes [34].

283 The formation of fullerenes in flames was earlier modeled with a gas-phase chemical network
284 taking into account competition between growth and destruction reactions [33,35]. These involved
285 the formation of pentagonal cycles by chemical reactivity as well as by thermal isomerization at the
286 flame temperatures. Homann [25] suggested that the chemistry can proceed via the formation of
287 aromers. Interestingly, our molecular analysis from just nucleated to the just-grown soot, allows us
288 to isolate two regimes. One in which there is a rich chemistry of PAHs leading to the formation of
289 large PAHs containing pentagonal cycles. Another one in which “carbonization” with a significant
290 hydrogen loss seems to govern the chemical evolution of the large carbonaceous molecules. It is

291 interesting to note that for $C_{\#} \geq 50$, fullerenes are observed at $Z=14$ mm but neither PAHs nor HC
292 clusters. For $C_{\#} < 50$, a much larger diversity of species are present with HC clusters spanning all
293 possible H numbers.

294 The transition from PAHs to fullerenes is an interesting topic in astrochemistry that leads to
295 experimental and modeling work [36,37]. Berné et al. [37] have evaluated in their photochemical
296 model, the possibility to convert $C_{66}H_{20}$ (i.e. circumovalene) into C_{60} fullerene upon irradiation by
297 ultraviolet photons. In this scenario, the formation of pentagonal cycles is expected after that PAH
298 has lost all its hydrogen atoms and the carbon cluster rearranges to fold into a fullerene structure,
299 while losing C_2 until it reaches the most stable fullerene structure of C_{60} . Although the authors
300 concluded about the viability of such a scenario in astrophysical environments, it relies on reaction
301 rates which are poorly constrained especially the ones concerning the folding process for which there
302 is no experimental data. From this study we can however keep the idea of a precursor “PAH-like”
303 population evolving towards fullerenes by energetic processing. In the oxidative environment of
304 flames, the formation of pentagonal cycles during the chemistry of formation of PAHs can favor the
305 formation of fullerene precursors. Further dehydrogenation and isomerization processes associated to
306 carbonization would then be the key step controlling the transition towards fullerenes. It is striking
307 that a simple calculation using Fig. 3 suggests that this process is very efficient. From $Z=8$ mm to
308 $Z=10$ mm, $1.2 \cdot 10^5$ (arbitrary units) large PAHs have been converted into $7 \cdot 10^3$ HC clusters and 1.6
309 10^4 fullerenes. An additional stock of $8.3 \cdot 10^4$ is available from $Z=10$ mm to $Z=14$ mm which would
310 lead proportionally to $5 \cdot 10^3$ HC clusters and $1.1 \cdot 10^4$ fullerenes. Assuming a similar detection
311 efficiency for both large HC clusters and fullerenes, we conclude that all these produced HC clusters
312 have been converted into fullerenes. The exact fraction of large PAHs that were converted into
313 fullerenes is difficult to assign because of the unknown relative detection efficiency between both
314 populations. Even without considering the detailed numbers, our work suggests that large PAHs are
315 converted into large HC clusters which efficiently produce fullerenes.

316

317 4. CONCLUSION

318 The molecular constituents of soot have been analyzed using two-steps laser desorption laser
319 ionization mass spectrometry in the transition zone from incipient to just-grown soot particles.

320 Fullerenes only appear in the last stage, which implies that they are not involved in soot nucleation.

321 From the analysis of the obtained mass spectra, we came to the following conclusions:

322 • Molecular constituents of incipient/just-nucleated soot (particles at $Z=8$ mm) are mostly
323 planar aromatics, not only *peri*-condensed but also in the form of less compact structures (more H
324 atoms with respect to the most *peri*-condensed PAHs) and of structures containing pentagonal cycles
325 (same number of H atoms or less with respect to the most *peri*-condensed PAHs). A large number of
326 radicals are also detected among these aromatic molecules mainly in the form of odd $C\#$ with odd $H\#$
327 corresponding to π radicals.;

328 • Just-grown soot particles ($Z = 14$ mm) contain a population of H-poorer molecules (less than
329 $49 C\#$), with a similar fraction of the population in radicals than for incipient soot. From sizes $50 C\#$
330 and above, only fullerenes are observed;

331 • The evolution of the molecular families within the nascent soot particle zone suggests an
332 efficient conversion of the large PAH population into fullerenes involving intermediate large HC
333 clusters with very fast evolution. This is consistent with a carbonization scheme in which thermal
334 processing induces a series of dehydrogenation and isomerization processes to form the fullerenes.

335

336 ACKNOWLEDGMENTS

337 This work was supported by the PRIN-project 2017PJ5XXX:-“MAGIC DUST”. The research leading
338 to these results has received funding from the European Research Council under the European
339 Union’s Seventh Framework Programme (FP/2007-2013) ERC-2013-SyG, Grant agreement
340 N°610256 NANOCOSMOS.

341

342 REFERENCES

- 343 [1] H. Wang, Formation of nascent soot and other condensed-phase materials in flames. *Proc.*
344 *Combust. Inst.* 33 (2011) 41-67.
- 345 [2] A. D'Anna, Combustion-formed nanoparticles. *Proc. Combust. Inst.* 32 (2009) 593-613.
- 346 [3] M. Commodo, G. De Falco, A. Bruno, C. Borriello, P. Minutolo, A. D'Anna, Physicochemical
347 evolution of nascent soot particles in a laminar premixed flame: from nucleation to early
348 growth. *Combust. Flame* 162 (2015) 3854-63.
- 349 [4] F. Carbone, M. Attoui, A. Gomez, Challenges of measuring nascent soot in flames as evidenced
350 by high resolution differential mobility analysis. *Aerosol Sci. Technol.* 50 (2016) 740-757.
- 351 [5] B. Zhao, Z. Yang, J. Wang, M.V. Johnston, H. Wang, Analysis of Soot Nanoparticles in a
352 Laminar Premixed Ethylene Flame by Scanning Mobility Particle Sizer, *Aerosol Sci. Technol.*
353 37 (2003) 611-620.
- 354 [6] M.M. Maricq, The dynamics of electrically charged soot particles in a premixed ethylene flame,
355 *Combust. Flame* 141 (2005) 406–416.
- 356 [7] R.A. Dobbins, Soot inception temperature and the carbonization rate of precursor particles.
357 *Combust. Flame* 130 (2002) 204–214.
- 358 [8] C. Russo, A. Tregrossi, A. Ciajolo, Dehydrogenation and growth of soot in premixed flames, /
359 *Proc. Combust. Institut.* 35 (2015) 1803–1809.
- 360 [9] K.A. Pratt, K.A. Prather, Mass spectrometry of atmospheric aerosols-Recent developments and
361 applications. Part I: Off-line mass spectrometry techniques, *Mass Spectrom. Rev.*, 31 (2012) 1-
362 16.
- 363 [10] K.A. Pratt, K.A. Prather, Mass spectrometry of atmospheric aerosols-Recent developments and
364 applications. Part II: On-line mass spectrometry techniques, *Mass Spectrom. Rev.*, 31 (2012)
365 17-48.
- 366 [11] R.S. Jacobson, A.R. Korte, A. Vertes, J.H. Miller, The Molecular Composition of Soot, *Angew.*
367 *Chem. Int. Ed.* 2020, 59, 4484 – 4490.
- 368 [12] O. Mathieu, G. Frache, N. Djebaili-Chaumeix, C.-E. Paillard, G. Krier, G., J.-F. Muller, F.
369 Douce, P. Manuelli, Laser desorption-ionization time-of-flight mass spectrometry for analyses
370 of heavy hydrocarbons adsorbed on soot formed behind reflected shock waves, *Proc. Combust.*
371 *Instit.* 32 (2009) 971-978.
- 372 [13] A. Faccinetto, P. Desgroux, M. Ziskind, E. Therssen, C. Focsa, High-sensitivity detection of
373 polycyclic aromatic hydrocarbons adsorbed onto soot particles using laser desorption/laser
374 ionization/time-of-flight mass spectrometry: An approach to studying the soot inception
375 process in low-pressure flames, *Combust. Flame* 158 (2011) 227–239.

- 376 [14] F. Schulz, M. Commodo, K. Kaiser, G. De Falco, P. Minutolo, G. Meyer, A. D'Anna, and L.
377 Gross. Insights into incipient soot formation by atomic force microscopy, *Proc. Combust. Inst.*
378 37 (2019) 885-892.
- 379 [15] M. Commodo, K. Kaiser, G. De Falco, P. Minutolo, F. Schulz, A. D'Anna, L. Gross, On the
380 early stages of soot formation: Molecular structure elucidation by high-resolution atomic force
381 microscopy, *Combust. Flame* 205 (2019) 154-164.
- 382 [16] H. Sabbah, A. Bonnamy, D. Papanastasiou, J. Cernicharo, J.-A. Martín-Gago, C. Joblin,
383 Identification of PAH Isomeric Structure in Cosmic Dust Analogs: The AROMA Setup,
384 *Astrophys. J.* 843:34 (2017).
- 385 [17] L. Martínez, G. Santoro, P. Merino, et al. Prevalence of non-aromatic carbonaceous molecules
386 in the inner regions of circumstellar envelopes. *Nat. Astron.* 4 (2020) 97-105.
- 387 [18] G. Santoro, L. Martínez, K. Lauwaet, M. Accolla, G. Tajuelo-Castilla, P. Merino, J.M. Sobrado,
388 R.J. Peláez, V.J. Herrero, I. Tanarro, A. Mayoral, M. Agúndez, H. Sabbah, C. Joblin, J.
389 Cernicharo, J.A. Martín-Gago (2020). The chemistry of cosmic dust analogues from C, C₂, and
390 C₂H₂ in C-rich circumstellar envelopes. arXiv preprint arXiv:2005.02902.
- 391 [19] J. Ahrens, M. Bachmann, Th. Baum, J. Griesheimer, R. Kovacs, P. Weilmünster, K.-H.
392 Homann, Fullerenes and their ions in hydrocarbon flames, *Int. J. Mass Spectrom.* 138 (1994)
393 133-148.
- 394 [20] T. Streibel, R. Zimmermann, Resonance-enhanced multiphoton ionization mass spectrometry
395 (REMPI-ms): Applications for process analysis, *Annu. Rev. Anal. Chem.* 7 (2014) 361-381.
- 396 [21] E.M. Adkins, J.A. Giaccai, J.H. Miller, Computed electronic structure of polynuclear aromatic
397 hydrocarbon agglomerates, *Proc. Combust. Inst.* 36 (2017) 957-964.
- 398 [22] B. Öktem, M.P. Tolocka, B. Zhao, H. Wang, M.V. Johnston, Chemical species associated with
399 the early stage of soot growth in a laminar premixed ethylene-oxygen-argon flame, *Combust.*
400 *Flame* 142 (2005) 364-373.
- 401 [23] H. Kietzmann, R. Rochow, G. Ganteför, W. Eberhardt, K. Vietze, G. Seifert, P. W. Fowler,
402 Electronic Structure of Small Fullerenes: Evidence for the High Stability of C₃₂, *Phys. Rev.*
403 *Lett.* 81 (1998) 5378-5381.
- 404 [24] R.A. Dobbins, R.A. Fletcher, H.-C. Chang, The evolution of soot precursor particles in a
405 diffusion flame, *Combust. Flame*, 115 (1998) 285-298.
- 406 [25] K.-H. Homann, Fullerenes and soot formation – new pathways to large particles in flames,
407 *Angew. Chem. Int. Ed.* 37 (1998) 2434-2451.

- 408 [26] M. Commodo, A. D'Anna, G. De Falco, R. Larciprete, P. Minutolo, Illuminating the earliest
409 stages of the soot formation by photoemission and Raman spectroscopy, *Combust. Flame* 181
410 (2017) 1339–1351.
- 411 [27] A.G. Marshall, R.P. Rodgers, *Petroleomics: Chemistry of the underworld*, *Proc. Natl. Acad.*
412 *Sci. USA* 105 (2008) 18090–18095.
- 413 [28] V.V. Lobodin, A.G. Marshall, C.S. Hsu, Compositional space boundaries for organic
414 compounds, *Anal. Chem.* 84 (2012) 3410–3416.
- 415 [29] J. Cain, A. Laskin, M.R. Kholghy, M.J. Thomson, H. Wang, Molecular characterization of
416 organic content of soot along the centerline of a coflow diffusion flame, *Phys. Chem. Chem.*
417 *Phys.* 16 (2014) 25862-25875.
- 418 [30] M. Frenklach, H. Wang, Detailed modeling of soot particle nucleation and growth. *Symp. (Int.)*
419 *Combust.* 23 (1991) 1559–1566.
- 420 [31] C. Joblin, C. Masselon, P. Boissel, P. de Parseval, S. Martinovic, J.-f. Muller Simulation of
421 Interstellar Aromatic Hydrocarbons Using Ion Cyclotron Resonance. Preliminary Results,
422 *Rapid Commun. Mass Spectrom.* 11 (1997) 1619-1623.
- 423 [32] M.J. Wornat, B.A. Vernaglia, A.L. Lafleur, E.F. Plummer, K. Taghizadeh, P.F. Nelson, C.-Z.
424 Li, A. Necula, L.T. Scott, Cyclopenta-fused polycyclic aromatic hydrocarbons from brown coal
425 pyrolysis, *Symp. Int. Combust.* 27 (1998) 1677-1680.
- 426 [33] C.J. Pope, J.B. Howard, Thermodynamic limitations for fullerene formation in flames,
427 *Tetrahedron*, 52 (1996) 5161-5178.
- 428 [34] H.Á. Galué, Decoding the infrared signatures of pyramidal carbons in graphenic molecular
429 nanostructures of interstellar origin, *Chem. Sci.*, 5 (2014) 2667-2676.
- 430 [35] J.B. Howard, L. Lafleur, Y. Makarovskiy, S. Mitra, C.J. Pope, T.K. Yadav, Fullerenes synthesis
431 in combustion, *Carbon* 30 (1992) 1183-1201.
- 432 [36] J. Zhen, P. Castellanos, D.M. Paardekooper, H. Linnartz, A.G.G.M. Tielens, Laboratory
433 Formation of Fullerenes from PAHs: Top-Down Interstellar Chemistry, *Astrophys. J.* 797
434 (2014) L30.
- 435 [37] O. Berné, J. Montillaud, C. Joblin, Top-down formation of fullerenes in the interstellar medium,
436 *Astron. Astrophys.* 577 (2015) A133.
- 437

438 **Figure Captions**

439

440 Fig.1. Mass spectra at three burner-to-probe distances, i.e., $Z = 8$ mm, $Z = 10$ mm and $Z = 14$ mm,
441 characteristic of the transition from incipient to just-grown soot particles. Fluences of $E_d = 150$
442 mJ/cm^2 and $E_i = 16 \text{ mJ}/\text{cm}^2$ have been used for the desorption (1064 nm) and ionization (266 nm)
443 lasers, respectively. Peak annotations are given for corresponding neutral species. Inset zoom graph
444 at $Z = 8$ mm presents some of the species detected over the (200-400) m/z range. At $Z = 10$ mm the
445 inset zoom graph shows the co-existence of aromatic species with carbon clusters. At $Z = 14$ mm the
446 inset zoom graph presents the detection of fullerenes over the (700-840) m/z range. ^{13}C isotopologs
447 are clearly seen in this zoom.

448

449 Fig.2. Colored map plots of DBE/ $C\#$ vs. carbon number ($C\#$) constructed from the molecular
450 formulas which have been derived from the mass spectra of soot sampled at $Z = 8, 10$ and 14 mm.
451 The color scale is representative of the relative intensity (normalized to the highest peak in the
452 spectrum) for each identified species. Black line refers to carbon clusters ($\text{DBE} = n(\text{C}) + 1$); green
453 line refers to the planar aromatic limit ($\text{DBE} = 0.9 * C\#$) [28], and magenta line refers to the purely
454 *peri*-condensed PAHs (most compact structures made of 6-member rings) with $\text{DBE} = -3.24 +$
455 $0.92 * C\#$.

456

457 Fig.3. Evolution of the molecular families derived from the mass spectra after DBE analysis.

458

459 Supplementary Materials for

460 **MOLECULAR CONTENT OF NASCENT SOOT: FAMILY**
461 **CHARACTERIZATION USING TWO-STEP LASER DESORPTION LASER**
462 **IONIZATION MASS SPECTROMETRY**

463
464 Hassan Sabbah ^a, Mario Commodo ^b, Francesca Picca ^c, Gianluigi de Falco ^c

465 Patrizia Minutolo ^b, Andrea D'Anna ^{c,*}, Christine Joblin ^{a,*}

466
467
468 ^a Institut de Recherche en Astrophysique et Planétologie (IRAP), Université de Toulouse (UPS),
469 CNRS, CNES, 9 Av. du Colonel Roche, 31028 Toulouse Cedex 4, France

470 ^b Istituto di Ricerche sulla Combustione, CNR, P.le Tecchio 80, 80125, Napoli, Italy

471 ^c Dipartimento di Ingegneria Chimica, dei Materiali e della Produzione Industriale - Università
472 degli Studi di Napoli Federico II, P.le Tecchio 80, 80125, Napoli, Italy

473
474
475
476
477
478
479
480
481 *** Corresponding Authors**

482 Andrea D'Anna anddanna@unina.it

483 Christine Joblin christine.joblin@irap.omp.eu

484

485

486

487 **AROMA capabilities to probe PAHs, carbon clusters and fullerenes from soot particles:**

488

489 Using the AROMA setup with a two-step laser mass spectrometry (L2MS) scheme (see Figure S1),
490 we showed the capability of the instrument to detect PAHs with high sensitivity (down to attomole)
491 and almost no fragmentation from pure PAHs and fullerenes C₆₀ samples¹. We reported experiments
492 in which the laser desorption fluence was varied by a factor of 20 and no aggregation nor
493 fragmentation was observed¹. We illustrated also our ability of detecting the PAH distribution in
494 Murchison meteorites and found a distribution similar to the one earlier published. In two recent
495 laboratory studies^{2,3} of the carbon chemistry in the dust formation zone of evolved stars, we have
496 shown that in the presence of C/C₂ and H₂, the formed dust samples contain C and HC clusters with
497 no fullerenes and only traces of aromatics, whereas with C₂H₂ added instead of H₂, PAHs are favored
498 but still with no fullerenes.

499

500 We applied the L2MS scheme to analyze the molecular constituents of the collected soot particles. In
501 the first step, a pulsed (5 ns) infrared laser (Nd:YAG at 1064 nm) is focused on the sample with a
502 spot size of 300 μm. This causes a high heating rate of 10¹¹-10¹² K/s, which favors desorption over
503 decomposition^{4,5}. The desorption laser fluence (E_d) and irradiance (I_d) used for this work are
504 respectively 150 mJ/cm² and 30 MW/cm². This fluence is one to two order of magnitudes lower than
505 the explosive vaporization threshold that results in plasma formation during ablation processes⁶. It is
506 also lower than the sublimation threshold (300 mJ/cm² for a 1064-nm laser) measured during laser-
507 induced incandescence (LII) experiments on soot particles^{7,8}. In these conditions, we do not observe
508 any signal from a highly-ordered pyrolytic graphite (HPOG) sample. We need to double the fluence
509 ($E_d = 300$ mJ/cm²) to start observing carbon clusters, with a distribution from C₁₀ to C₂₅. In our
510 conditions, no fullerenes are generated even for E_d as high as 1 J/cm². In the second step, a pulsed (5
511 ns) ultraviolet laser (fourth harmonic of an Nd:YAG at 266 nm) intercepts perpendicularly the
512 expanding plume of the desorbed molecules. This leads to selectively ionize fullerene and aromatic
513 species that are present in the plume and can undergo (1+1) resonance-enhanced multiphoton
514 ionization (REMPI). The ionization laser fluence (E_i) and irradiance (I_i) used for this work are
515 respectively 16 mJ/cm² and 3 MW/cm². These values fit in the range reported to correctly probe PAHs
516 in soot collected particles⁹. The laser energy per pulse is optimized to have parent ions and not
517 fragments dominating the mass spectra. Ions produced at low pressure (10⁻⁶ mbar) are collimated by
518 a set of DC high-voltage lenses and are thermalized in a radio-frequency (RF) octapole. Generated
519 ions are then monitored with the orthogonal time of flight mass spectrometer (oTOF). For each m/z
520 range scan, the amplitude and RF frequency applied on the electrodes of the linear quadrupole ion
521 trap (LQIT) are optimized to maximize ion signal in this mass range. Each scan is the result of 50
522 laser shots. The interaction of the desorption laser with the sample is controlled with a mechanical
523 shutter. The laser hits the sample once every 2 seconds. The sample is then moved so that the next
524 laser shot hits a fresh spot.

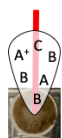
525

526 Laser desorption mass spectrometry techniques are powerful tools and are widely used to analyze
527 complex hydrocarbon mixtures with high sensitivity, selectivity and microscale spatial resolution<sup>9-
528 12</sup>. In addition of L2MS, single laser desorption/ionization (LDI) (with or without matrix) is often
529 used. Laser desorption irradiance in L2MS is much lower than in LDI^{13,14}. This gives L2MS higher
530 sensitivity and reduce substantially fragmentation as well as eliminate aggregation in the expanding
531 plume¹⁵⁻¹⁷. LDI and L2MS have been widely used to analyze molecular contents of soot samples^{10,18}.
532 REMPI in the ultraviolet (UV) domain is the most used technique in the L2MS scheme to probe
533 aromatics down to sub-femtomoles sensitivity levels¹⁹. It is also employed in flame studies to detect
534 neutral large aromatics and fullerenes^{20,21}.

535
536
537

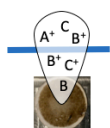
AROMA setup with the L2MS scheme:

1. Pulsed IR laser desorption ($\lambda=1064$ nm), Pulse duration = 5 ns, $E_d=150$ mJ/cm²

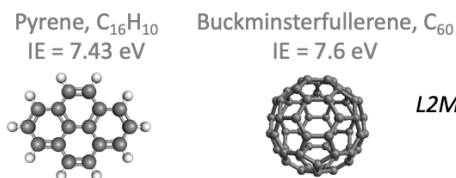


- plume dominated by neutral molecules
- heating rates of 10^8 K.s⁻¹
- this favors desorption process over decomposition

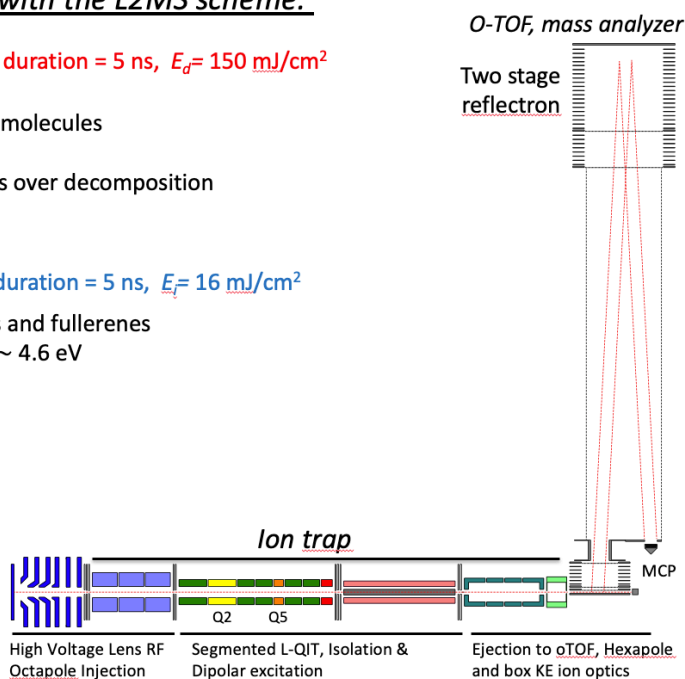
2. Pulsed UV laser ionization ($\lambda=266$ nm), Pulse duration = 5 ns, $E_i=16$ mJ/cm²



- 1+1 REMPI to ionize aromatics and fullerenes
- ionization energy per photon ~ 4.6 eV



L2MS ion source



538
539
540
541
542
543
544

Fig. S1. Schematic diagram of the AROMA setup highlighting the L2MS principle and the principal components of the instrument.

545 **Particle size distribution:**

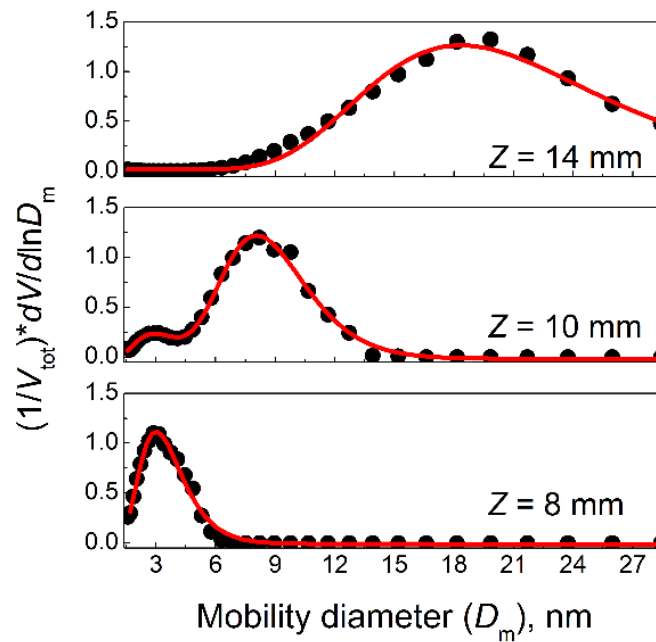
546

547 Particle size distribution (PSD) were measured in a previous study²². The data are reported as
548 normalized volumetric particle distributions in Fig. S2 for the three sampling conditions investigated
549 in the current study using the AROMA setup. For PSD measurements, a differential mobility analyzer
550 (DMA) was used: the aerosol sample passed through an X-ray charger (TSI Model-3088) first, and
551 was then selected in an electrostatic classifier (DMA Model-TapCon 3/150), and counted by a
552 Faraday cup electrometer²².

553

554

555



556

557

558 Fig. S2. PSDs at the three selected probe-to-burner distances, i.e., $Z = 8$ mm, $Z = 10$ mm, and $Z = 14$
559 mm, characteristic of the transition from incipient to primary soot particles. Black dots are
560 experimental data by DMA measurements; red lines are the results of the lognormal fit.

561

562

563 **DBE method and family analysis:**

564

565 For each detected m/z peak with a signal-to-noise ratio (S/N) greater than 10, a chemical formula is
566 assigned using the mMass software²³, an open source mass spectrometry tool. We then calculate the
567 double bond equivalent (DBE) for each molecular formula. The DBE value is defined by $DBE = C\#$
568 $- H\#/2 + N\#/2 + 1$ with C#, H# and N#, the numbers of C, H and N atoms inside the molecules. The
569 DBE is equal to the number of rings plus double bonds involving carbon atoms (because each ring or
570 double bond results in a loss of two hydrogen atoms). An increasing number of H atoms in a molecule
571 decreases unsaturation and hence leads to lower DBE values. The DBE method is used, for example,
572 in petroleomics to separate and sort petroleum components²⁴. Empirical factors²⁵ and DBE
573 boundaries²⁶ have been set for hydrocarbons to contain or not aromatic moieties in complex natural
574 organic matter. This method allows us to sort the detected ions into families of compounds.

575

576

577

578

579

580

581

582

583

584

585

586

587

588

589

590

591

592

593

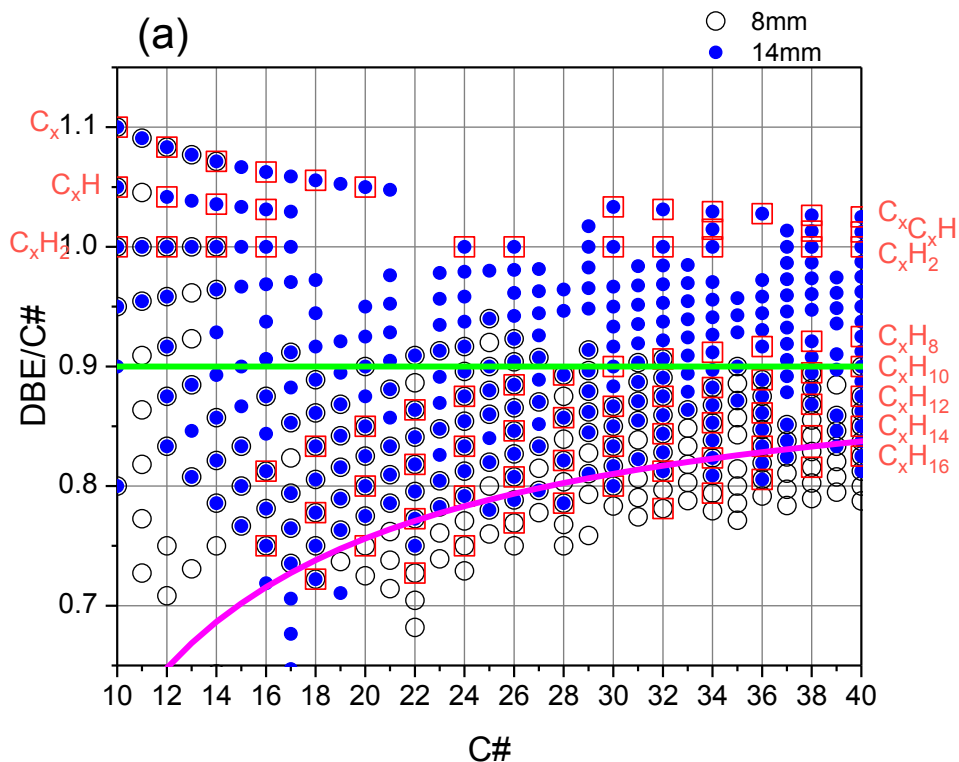
594

595

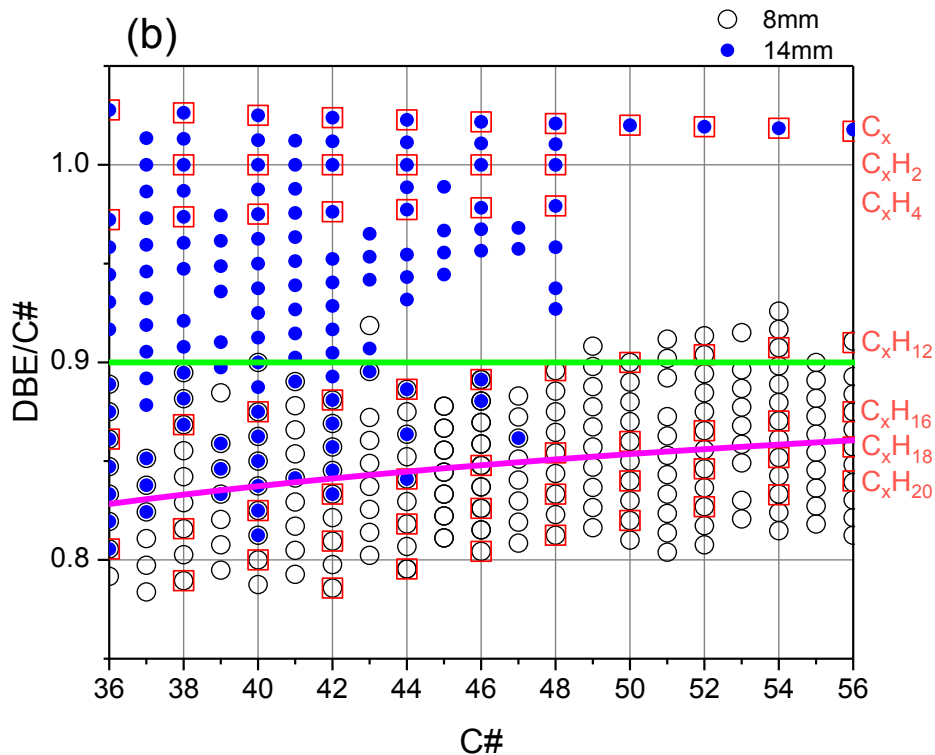
596

597

598 **DBE/C# vs C# for soot samples collected at Z = 8 mm and 14 mm**



599



600

601 Fig. S3 DBE/C# vs. number of carbon atoms plots for all detected species in samples Z = 8 mm and

602 14 mm: (a) C# from 10 to 40; (b) C# from 36 to 56. Red squares surrounding the symbols in the

603 figure indicate the sequences of C# for a fixed number of H as indicated in the formulas on the side

604 of each graph. Green and magenta curves show the aromatic limits as defined in Fig. 2 in the
605 manuscript.

606
607
608
609
610
611
612
613
614
615
616
617
618
619
620
621
622
623
624
625
626
627
628
629
630
631
632
633
634
635
636
637
638
639
640
641
642
643
644
645
646
647
648
649
650
651
652
653
654
655
656

References:

1. Sabbah, H. *et al.* Identification of PAH Isomeric Structure in Cosmic Dust Analogs : The AROMA Setup. *Astrophys. J.* **843**, (2017).
2. Martínez, L. *et al.* Prevalence of non-aromatic carbonaceous molecules in the inner regions of circumstellar envelopes. *Nat. Astron.* **4**, 97–105 (2020).
3. Santoro, G. *et al.* The chemistry of cosmic dust analogues from C, C₂, and C₂H₂ in C-rich circumstellar envelopes. (2020).
4. Deckert, A. A. & George, S. M. Heating Rates Required for Laser Induced Thermal Desorption Studies of Surface Reaction Kinetics. *Surf. Sci.* **182**, 215–220 (1987).
5. Zare, R. & Levine, R. Mechanism for bond-selective processes in laser desorption. *Chem. Phys. Lett.* **136**, 593–599 (1987).
6. Hoffman, J. *et al.* The effect of laser wavelength on the ablation rate of carbon. *Appl. Phys. A Mater. Sci. Process.* **117**, 395–400 (2014).
7. Goulay, F., Schrader, P. E. & Michelsen, H. A. Effect of the wavelength dependence of the emissivity on inferred soot temperatures measured by spectrally resolved laser-induced incandescence. *Appl. Phys. B Lasers Opt.* **100**, 655–663 (2010).
8. Johansson, K. O., El Gabaly, F., Schrader, P. E., Campbell, M. F. & Michelsen, H. A. Evolution of maturity levels of the particle surface and bulk during soot growth and oxidation in a flame. *Aerosol Sci. Technol.* **51**, 1333–1344 (2017).
9. Faccinnetto, A., Desgroux, P., Ziskind, M., Therssen, E. & Focsa, C. High-sensitivity detection of polycyclic aromatic hydrocarbons adsorbed onto soot particles using laser desorption/laser ionization/time-of-flight mass spectrometry: An approach to studying the soot inception process in low-pressure flames. *Combust. Flame* **158**, 227–239 (2011).
10. Mathieu, O. *et al.* Laser desorption-ionization time-of-flight mass spectrometry for analyses of heavy hydrocarbons adsorbed on soot formed behind reflected shock waves. *Proc. Combust. Inst.* **32 I**, 971–978 (2009).
11. Sabbah, H. *et al.* Comparing laser desorption/Laser ionization mass spectra of asphaltenes and model compounds. *Energy and Fuels* **24**, (2010).
12. Sabbah, H., Morrow, A. L., Pomerantz, A. E. & Zare, R. N. Evidence for Island Structures as the Dominant Architecture of Asphaltenes. *Energy & Fuels* **25**, 1597–1604 (2011).
13. Getty, S. a. 42nd Lunar and Planetary Science Conference (2011) 42nd Lunar and Planetary Science Conference (2011). 1–2 (2011).
14. Getty, S. a, Brinckerhoff, W. B., Cornish, T., Ecelberger, S. & Floyd, M. Compact two-step laser time-of-flight mass spectrometer for in situ analyses of aromatic organics on planetary missions. *Rapid Commun. Mass Spectrom.* **26**, 2786–90 (2012).
15. Pomerantz, A. E., Hammond, M. R., Morrow, A. L., Mullins, O. C. & Zare, R. N. Two-Step Laser Mass Spectrometry of Asphaltenes. *J. Am. Chem. Soc.* **130**, 7216–7217 (2008).
16. Hortal, A. R., Hurtado, P., Martínez-Haya, B. & Mullins, O. C. Molecular-weight distributions of coal and petroleum asphaltenes from laser desorption/ionization experiments. *Energy and Fuels* **21**, 2863–2868 (2007).
17. Hurtado, P., Gámez, F. & Martínez-Haya, B. One- and Two-Step Ultraviolet and Infrared Laser Desorption Ionization Mass Spectrometry of Asphaltenes. *Energy & Fuels* **24**, 6067–6073 (2010).
18. FACCINETTO, A., Thomson, K., Ziskind, M. & Focsa, C. Coupling of desorption and photoionization processes in two-step laser mass spectrometry of polycyclic aromatic hydrocarbons. *Appl. Phys. A* **92**, 969–974 (2008).
19. Hahn, J. H., Zenobi, R. & Zare, R. N. Subfemtomole quantitation of molecular adsorbates by two-step laser mass spectrometry. *J. Am. Chem. Soc.* **109**, 2842–2843 (1987).
20. Ahrens, J., Kovacs, R., Shafranovskii, E. A. & Homann, K. H. On-line multi-photon ionization mass spectrometry applied to PAH and fullerenes in flames. *Berichte der*

- 657 *Bunsengesellschaft für Phys. Chemie* **98**, 265–268 (1994).
- 658 21. Streibel, T. & Zimmermann, R. Resonance-Enhanced Multiphoton Ionization Mass
659 Spectrometry (REMPI-MS): Applications for Process Analysis. *Annu. Rev. Anal. Chem.* **7**,
660 361–381 (2014).
- 661 22. Commodo, M. *et al.* On the early stages of soot formation: Molecular structure elucidation
662 by high-resolution atomic force microscopy. *Combust. Flame* **205**, 154–164 (2019).
- 663 23. Strohalm, M., Kavan, D., Novák, P., Volný, M. & Havlíček, V. MMass 3: A cross-platform
664 software environment for precise analysis of mass spectrometric data. *Anal. Chem.* **82**, 4648–
665 4651 (2010).
- 666 24. Marshall, A. G. & Rodgers, R. P. Petroleomics : Chemistry of the underworld. *PNAS* **2008**,
667 (2008).
- 668 25. Koch, B. P. & Dittmar, T. From mass to structure : an aromaticity index for high-resolution
669 mass data of natural organic matter. 926–932 (2006) doi:10.1002/rcm.2386.
- 670 26. Hsu, C. S., Lobodin, V. V., Rodgers, R. P., McKenna, A. M. & Marshall, A. G.
671 Compositional boundaries for fossil hydrocarbons. *Energy and Fuels* **25**, 2174–2178 (2011).
672